# We are IntechOpen,
# the world's leading publisher of
# Open Access books
# Built by scientists, for scientists

## 5,500
Open access books available

## 136,000
International authors and editors

## 170M
Downloads

## 154
Countries delivered to

Our authors are among the

## TOP 1%
most cited scientists

## 12.2%
Contributors from top 500 universities

CLARIVATE ANALYTICS

BOOK
CITATION
INDEX

INDEXED

**WEB OF SCIENCE**™

Selection of our books indexed in the Book Citation Index
in Web of Science™ Core Collection (BKCI)

## Interested in publishing with us?
## Contact book.department@intechopen.com

Chapter

# Magnesium containing High Entropy Alloys

*Prince Sharma, Nushrat Naushin, Sahil Rohila and Abhishek Tiwari*

## Abstract

High Entropy alloys (HEAs) or Complex Concentrated Alloys (CCAs) or Multi-Principal Element Alloys (MPEAs) is a matter of interest to material scientists for the last two decades due to the excellent mechanical properties, oxidation and corrosion resistant behaviors. One of the major drawbacks of HEAs is their high density. Mg containing HEAs show low density compared to peers, although extensive research is required in this field. This chapter aims to include all the available information on synthesis, design, microstructures and mechanical properties of Mg containing HEAs and to highlight the contemporary voids that are to be filled in near future.

**Keywords:** Magnesium, High Entropy Alloys, Light Weight Alloys, Microstructure, Mechanical Properties

## 1. Introduction

The ancient strategy of alloy design and production has been followed for a long period and it will remain a crucial part of industry. The strategy is based on one principal element solvent with solute elements dissolved in the lattice either as heterogeneities or precipitate particles. Although, ancient Indian scriptures in Sanskrit mentions the existence of multi principal alloys named as "Tri-loh" (loh means Iron), "Panch-dhatu" and "Asht-dhatu" in which Tri, Panch and Asht mean three, five and eight respectively [1]. These dhatus or metals were used for special and sacred purposes such as making idols, deities and machines [2]. The context of these alloys can be found in books and Sanskrit text titled "Vimanika Shastra", "Ras-Ratnakar-Samuchaya", "Shilparatna", "Manasara", "Ras-Tarangini", and "Ras-grandhas". These alloys were used for special purposes and the knowledge of their synthesis was mostly limited to the *Sages* and *Rishis*, which has never been researched and explored by the scientific community. The concept of multi principal element or high entropy alloy is modern version of the "Panch-dhatu".

The concept of maximization of configurational entropy by using five or more elements in nearly equi-atomic composition has revolutionized the field of alloy design and metallurgy. The first scientific report of such alloys were reported independently by Cantor et. al. and Yeh et. al [3, 4]. HEAs show better mechanical, oxidation, corrosion and irradiation properties compared to commercial alloys. HEAs show four key effects and a postulate, which are: high-entropy effect, severe lattice distortion, sluggish diffusion, short range order effect and cocktail effect [5].

## 2. Scope of this chapter

The authors aimed to present detailed review and analysis of design, synthesis, microstructures and mechanical properties of Mg containing MPEAs from all the existing scientific articles on the topic available to this date. The presence of multiple principal elements in an alloy makes it difficult to interpret the reasons behind the behavior of HEAs. This study presents the possible interpretations of the structure-properties-processing relationship of Mg containing alloys in both equiatomic and non-equiatomic compositions. **Figure 1** shows the gradual increase in interest in Mg-HEAs.
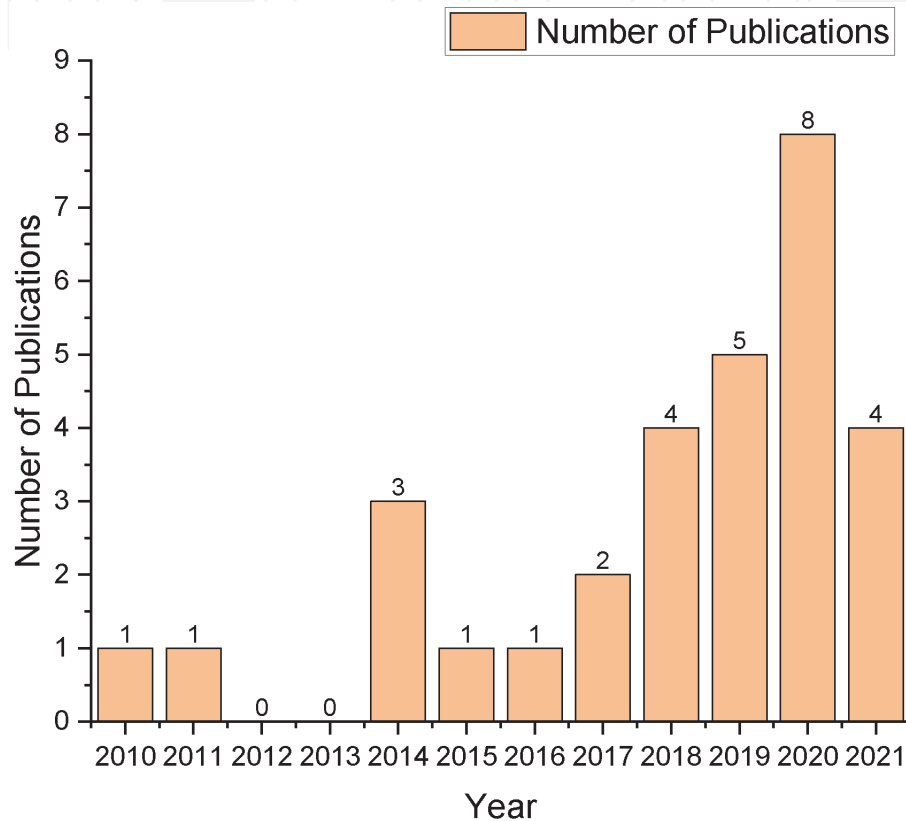


**Figure 1.**
*Year vs number of publications of Mg containing HEAs.*

## 3. Basics of HEAs

HEAs are multicomponent systems containing five or more elements in significant proportions unlike conventional alloys [6]. This leads to increase in the overall configurational entropy of system, which was first reported by Yeh et. al. for CuCoNiCrAlFe system [4]. It was believed that due to high configurational entropy of mixture, the alloys tend to crystallize as SS instead of intermetallic compounds (IM). These compositions exhibit superior mechanical, oxidation and corrosion resistance properties under conditions ranging from high temperatures to cryogenic temperatures [5, 6]. Due to the prominence of high entropy effect in multi-principal element alloys, such alloys are commonly referred as high entropy alloys. There are four core effects and one postulate, as follows:

### 3.1 The high entropy effect

The name perhaps has gathered enormous attention of researchers in this system. It states that high configurational entropy of mixing ($\Delta S_{conf}$) supports the

formation of SS instead of IM [4]. This also limits the number of phases predicted by the Gibbs Phase Rule. $\Delta S_{conf}$ is given by Eq. (1),

$$\Delta S_{conf} = -R \sum_{i=1}^{n} X_i \ln X_i \qquad (1)$$

On dealing with this phenomenon on the grounds of probability, the possible explanation of absence of IM is in the basic nature of these compounds. Intermetallics are strictly ordered in nature but in case of HEAs, there is interaction with various elements with significantly higher compositions. As a result, even if thermodynamic and kinetic factors favor compound formation, the probability of tendency to form a two elements compound being in vicinity, is reduced. Intermetallics (IMs) are established by a high value of negative enthalpy of mixing ($\Delta H_{mix}$) and so entropy maximization plays an important role in lowering the Gibbs free energy of mixing and promoting SS formation. Here, $\Delta H_{mix}$ Denotes enthalpy of mixing of all elements and is given by Eq. (2). In cases, where $\Delta H_{mix}$ of an intermetallic is higher compared to the solid solution phases, there is formation of IM and SS together. The $\Omega$ factor introduced by Yang and Zhang [7], should ideally be greater than 1.1 to stabilize the SS.

$$\Delta H_{mix} = \sum_{i=1, j>1}^{n} 4\Delta H_{AB}^{mix} c_i c_j \qquad (2)$$

$$\Omega = \frac{T_m \Delta S_{conf}}{|\Delta H_{mix}|} \qquad (3)$$

$$T_m = \sum_{i=1}^{n} T_i c_i$$

## 3.2 The lattice distortion effect

Unlike conventional alloys with a single element solvent matrix, the HEAs comprises of a random solute matrix (RSM). The assumption, that RSM comprises of constituting elements arranged with complete disordered fashion and hence result in a SS, is mostly true. There is occasional occurrence of some intermetallic phases in the alloy which could be due to (a) enthalpy of formation of intermetallic is very high compared to the enthalpy of mixture; (b) the difference in atomic size is less (1.1-1.6) which supports formation of ordered structure; (c) the incorporation of elements with very small atoms in the alloy, which forms interstitial compounds. The Lattice Distortion Effect (LDE) is theoretically estimated by polydisparity or atomic mismatch factor δ given by Eq. (4) [7].

$$\delta = \sqrt{\sum_{i=1}^{n} c_i \left(1 - \frac{r_i}{\sum_{j=1}^{n} c_j r_j}\right)^2} \qquad (4)$$

The LDE tends to increase the hardness of HEAs because of solution hardening.

## 3.3 The sluggish diffusion hypothesis

Studies suggest that MPEAs exhibit a diffusion rate slower than any regular alloys and which could be responsible for the lower number of phases present in MPEAs [8]. This slow diffusion behaviour is claimed as sluggish diffusion. The HEAs studied at the beginning exhibited this behavior, though the sluggish

| Sr. No. | HEA Composition | Mg | Phases | Tm (K) | $\Delta S/R$ | VEC | $\delta$ | $\Delta\chi$ | $\Delta H$ (KJmol$^{-1}$) | $\Omega$ | Density |
|---|---|---|---|---|---|---|---|---|---|---|---|
| 1 | $Al_8Li_{0.5}Mg_{0.5}Sn_{0.5}Zn_{0.5}$ | 0.05 | SS + IM | 875.55 | 0.78 | 3.35 | 0.0398 | 0.17 | −0.54 | 10.48 | 3.05 |
| 2 | $Al_8Cu_{0.5}Li_{0.5}Mg_{0.5}Zn_{0.5}$ | 0.05 | SS + IM | 918.18 | 0.78 | 3.70 | 0.0424 | 0.17 | −1.15 | 5.16 | 3.08 |
| 3 | $Al_{60}Cu_{10}Fe_{10}Cr_5Mn_5Ni_5Mg_5$ | 0.05 | SS + IM | 1191.78 | 1.37 | 4.95 | 0.0736 | 0.14 | −7.91 | 1.71 | 4.6 |
| 4 | $Al_{35}Cr_{14}Mg_6Ti_{35}V_{10}$ | 0.06 | SS | 1281.16 | 1.13 | 3.07 | 0.1561 | 0.22 | −15.49 | 0.78 | 4.05 |
| 5 | $Al_{20}Li_{20}Mg_{10}Sc_{20}Ti_{30}$ | 0.10 | SS | 1315.04 | 1.56 | 2.80 | 0.0455 | 0.23 | −0.40 | 42.56 | 2.67 |
| 6 | $Mg_{0.10}Ti_{0.30}V_{0.25}Zr_{0.10}Nb_{0.25}$ | 0.10 | SS + IM | 2208.40 | 1.56 | 4.74 | 0.0722 | 0.12 | 6.08 | 4.71 | NA |
| 7 | $AlFeCuCrMg_{0.5}$ | 0.11 | SS | 1487.12 | 1.58 | 6.44 | 0.08 | 0.18 | 4.05 | 4.83 | 5.79 |
| 8 | $MgMoNbFeTi_2$ | 0.17 | SS | 2042.21 | 1.56 | 4.83 | 0.0662 | 0.27 | 6.22 | 4.26 | NA |
| 9 | $MgMoNbFeTi_2Y_{0.004}$ | 0.17 | SS | 2041.98 | 1.56 | 4.83 | 0.0662 | 0.27 | 6.22 | 4.26 | NA |
| 10 | $MgMoNbFeTi_2Y_{0.008}$ | 0.17 | SS | 2041.99 | 1.56 | 4.83 | 0.0662 | 0.27 | 6.22 | 4.26 | NA |
| 11 | $MgMoNbFeTi_2Y_{0.012}$ | 0.17 | SS | 2042.00 | 1.56 | 4.83 | 0.0662 | 0.27 | 6.22 | 4.26 | NA |
| 12 | AlLlMgSnZn | 0.20 | SS + IM | 701.63 | 1.61 | 4.40 | 0.0611 | 0.33 | −6.24 | 1.50 | 4.23 |
| 13 | AlFeCuCrMg | 0.20 | SS + IM | 1430.84 | 1.61 | 6.00 | 0.0925 | 0.21 | 6.24 | 3.07 | 5.37 |
| 14 | $Mg_{20}(MnAlZnCu)_{80}$ | 0.20 | SS + IM | 1084.80 | 1.61 | 7.00 | 0.117 | 0.19 | −3.04 | 4.77 | 4.29 |
| 15 | MgVAlCrNi | 0.20 | SS | 1154.90 | 1.29 | 4.00 | 0.2335 | 0.35 | −6.24 | 1.98 | NA |
| 16 | MgAlSiCrFe | 0.20 | SS + IM | 1159.30 | 1.29 | 3.80 | 0.2473 | 0.33 | 2.88 | 4.31 | NA |
| 17 | Al2MgLiCa | 0.20 | IM | 873.35 | 1.33 | 2.20 | 0.1302 | 0.28 | −9.44 | 1.02 | NA |
| 18 | MgVAlCr | 0.25 | SS | 1544.13 | 1.39 | 4.00 | 0.0832 | 0.14 | 4.25 | 4.19 | NA |
| 19 | MgVAlNi | 0.25 | SS | 1443.63 | 1.39 | 5.00 | 0.0602 | 0.21 | −9.75 | 1.71 | NA |
| 20 | MgVCrNi | 0.25 | SS | 1742.75 | 1.39 | 5.75 | 0.0861 | 0.21 | 4.00 | 5.02 | NA |
| 21 | AlMgLiCa | 0.25 | IM | 858.30 | 1.39 | 2.00 | 0.1285 | 0.26 | −8.25 | 1.20 | NA |
| 22 | $Mg_{26}V_{31}Al_{31}Cr_6Ni_6$ | 0.26 | SS | 1439.75 | 1.41 | 3.96 | 0.0703 | 0.16 | −2.10 | 8.05 | NA |

| Sr. No. | HEA Composition | Mg | Phases | Tm (K) | $\Delta S/R$ | VEC | $\delta$ | $\Delta\chi$ | $\Delta H$ (KJmol$^{-1}$) | $\Omega$ | Density |
|---|---|---|---|---|---|---|---|---|---|---|---|
| 23 | $Mg_{28}V_{28}Al_{19}Cr_{19}Ni_6$ | 0.28 | SS | 1557.39 | 1.51 | 4.27 | 0.0826 | 0.17 | 3.82 | 5.13 | NA |
| 24 | $AlFeCuCrMg_{1.7}$ | 0.30 | SS + IM | 1368.19 | 1.58 | 5.51 | 0.1 | 0.22 | 7.99 | 2.25 | 4.91 |
| 25 | $AlMgLiCa_{0.3}$ | 0.30 | IM | 802.19 | 1.30 | 2.00 | 0.0962 | 0.26 | −5.18 | 1.68 | NA |
| 26 | $AlLi_{0.5}MgSn_{0.2}Zn_{0.5}$ | 0.31 | SS + IM | 790.87 | 1.48 | 3.84 | 0.061 | 0.27 | −3.98 | 2.44 | 3.22 |
| 27 | $AlCu_{0.2}Li_{0.5}MgZn_{0.5}$ | 0.31 | IM | 844.16 | 1.48 | 4.28 | 0.0702 | 0.26 | −3.40 | 3.06 | 3.73 |
| 28 | $AlCu_{0.5}Li_{0.5}MgSn_{0.2}$ | 0.31 | SS + IM | 894.76 | 1.48 | 3.69 | 0.0774 | 0.31 | −3.65 | 3.02 | 3.69 |
| 29 | $Mg_{33}(MnAlZnCu)_{67}$ | 0.33 | SS + IM | 1058.51 | 1.56 | 8.03 | 0.2294 | 0.45 | −3.69 | 3.72 | 3.41 |
| 30 | $Mg_{35}Al_{33}Li_{15}Zn_7Ca_5Cu_5$ | 0.35 | SS + IM | 893.96 | 1.50 | 2.93 | 0.1339 | 0.24 | −7.44 | 1.50 | 2.25 |
| 31 | $Mg_{35}Al_{33}Li_{15}Zn_7Ca_5Cu_5$ | 0.35 | SS + IM | 871.70 | 1.50 | 3.33 | 0.1091 | 0.26 | −4.97 | 2.19 | 2.27 |
| 32 | $Mg_{43}(MnAlZnCu)_{57}$ | 0.43 | SS + IM | 1038.29 | 1.47 | 5.56 | 0.1209 | 0.21 | −1.38 | 9.22 | 2.71 |
| 33 | $Mg_{45.6}(MnAlZnCu)_{54.4}$ | 0.46 | SS + IM | 1033.03 | 1.44 | 5.40 | 0.12 | 0.21 | −1.23 | 10.07 | 2.53 |
| 34 | $Mg_{50}(MnAlZnCu)_{50}$ | 0.50 | SS + IM | 1024.13 | 1.39 | 5.13 | 0.1181 | 0.21 | −1.00 | 11.80 | 2.2 |
| 35 | $Mg_{80}Al_5Cu_5Mn_5Zn_5$ | 0.80 | SS + IM | 963.45 | 0.78 | 3.25 | 0.085 | 0.16 | −0.04 | 155.73 | 1.74 |

**Table 1**
*Value of empirical parameters of Mg containing HEAs.*

diffusion is not entirely common for every HEA. Depending upon the alloy composition, the behavior varies [9]. The diffusion studies have been conducted in a limited number of alloys. Earlier studies on CoCrFeMnNi at near $T_m$ temperatures exhibit sluggish diffusion as per diffusion couple method and quasi binary path [10, 11]. A few studies suggest that the diffusion is not sluggish in CoCrFeMnNi within 1073K-1373K temperature range, when analyzed with Radiotracer method using $^{63}Ni$. Bulk diffusion is the prominent mode of diffusion in a single crystal CoCrFeMnNi, while bulk diffusion is also in polycrystalline alloys at high temperatures [9]. Using Boltzman-Matano method to study diffusion behaviour also reveals similar results [12]. Radiotracer method using $^{51}Cr$, $^{54}Mn$, $^{57}Cr$, $^{59}Fe$ and $^{63}Ni$ in the same alloy also produced similar non-sluggish diffusion behaviour when analyzed at a temperature range of 1073K-1373K [13–17]. AlCoCrFeNi HEAs exhibit sluggish diffusion behaviour when analyzed using diffusion couple method [18]. Numerical assessments also suggest similar behaviour. Another study on $Al_x CoCrCuFeNi$ where x=1, 1.5, 1.8 suggests that the diffusion retards with increasing the Al-concentration [19].

### 3.4 The Cocktail effect

Cocktail effect is a postulate, first identified by Prof. S. Ranganathan [20]. It refers to the unpredictable improvement in properties of materials based on the synergy of multi principal alloying elements. The properties range from near zero thermal expansion, ultra-high strength, corrosion resistance, good fracture toughness, ductility to photovoltaic effects or thermo-electronic responses [5]. This effect reminds about the acceptance of unique properties formed due to unusual combinations of elements as observed in MPEAs.

### 3.5 The short-range ordering

Besides these effects, chemical short range ordering (CSRO) has a significant impact on the mechanical properties, as it is proved to facilitate phase transformations in HEAs [21]. The CSRO has direct correlation with the activation energy of phase transformation from FCC to HCP phase in CoCrNi alloys [22]. The presence of SRO increases the Stacking Fault Energy (SFE) and yield strength in several alloys; it has been proved for CoCrNi alloys both experimentally and computationally [21–23]. A study using reverse Monte-Carlo suggests that the presence of SRO in TiVNb alloys is responsible for forming the FCC supercells in the alloy [21, 24].
All the empirical parameters discussed in above sections are calculated on the basis of available information in **Table 1**.

## 4. Why Mg HEAs

Since the inception, there have been several doubts, questions and strong arguments against HEAs. Most of them are related to scalability and process engineering in industries, repeatability, reliability, applications and high density of HEAs. Among all these drawbacks, process engineering of HEAs is least studied, while the major problem are repeatability and their high density. To obtain a high level of repeatability, an extensive standard of alloy preparation and their further processing must be established throughout the world. The problem of high density is being solved with the development of light weight HEAs (LHEA) containing low density elements such as Al, Ti, Li and Mg. LHEAs consisting of Mg and Li are

found to be lightest [25]. Mg based alloys have several applications in aircraft and automobile panels, bio-implants and energy storage. Mg alloys show exceptional and beautiful microstructures with Long Period Stacking Order (LPSO) phases. LPSO phases are most important feature of few Mg based alloys systems Mg-TM-RE (TM: transition metal, RE: rare earth metal) alloy as it enhances the mechanical properties at room and elevated temperatures [26]. *LPSO phases are not yet reported in Mg-HEAs and could be one of the most interesting breakthrough in Light-weight High Entropy Alloys (LHEAs).*

There are several other factors which makes Mg-HEAs a topic of interest for example, Magnesium alloy anodes tends to increase the efficiency of Mg-ion batteries which may replace Li-ion batteries in future; Mg is a fast biodegradable and bio-compatible material. Magnesium alloys do not possess enough strength compared to the bone tissue. Mg containing HEAs could be the answer to this problem. Lynette W. Cheah found that for every 10 % mass reduction in vehicle, fuel consumption may reduce by 7 % [27]. If the parts of vehicle are made of strong alloys containing Mg and/or Al instead of Iron, the weight reduction will be 45 and 29 % respectively. This will significantly lower the carbon emission and save fossil fuel. The disadvantage with high reactivity of Mg and low strength of its alloys can be avoided by the virtue of introducing severe lattice distortion, high entropy effect and cocktail effect. This means that Mg must be alloyed with three or more elements to increase the configurational entropy of alloy to attain higher stability and strength.

Clearly, Mg containing HEAs are materials for future.

Alloying has a positive impact on the properties of Mg, and it has been proven that Al addition increases hardness, strength and castability without significantly affecting the density [28]. Ca enhances the thermo-mechanical properties, increases creep resistance and refines the grains. Nd and Ni both increase the strength of Mg when added separately. Cu enhances mechanical properties and aid thermal stability. Ce addition improves corrosion resistance; Mn increases saltwater corrosion resistance in Mg-Al alloys; Zn increases corrosion resistance in Mg-Ni-Fe alloys; Sn prevents cracks during Mg-Al alloy processing and Sr increases creep resistance [28, 29]. Every element has a unique effect on alloy, as shown in **Figure 2** and hence, HEAs must be exploited to establish a synergy between different alloying elements in Mg to produce an alloy with high strength to weigh ratio. In **Figure 2**,
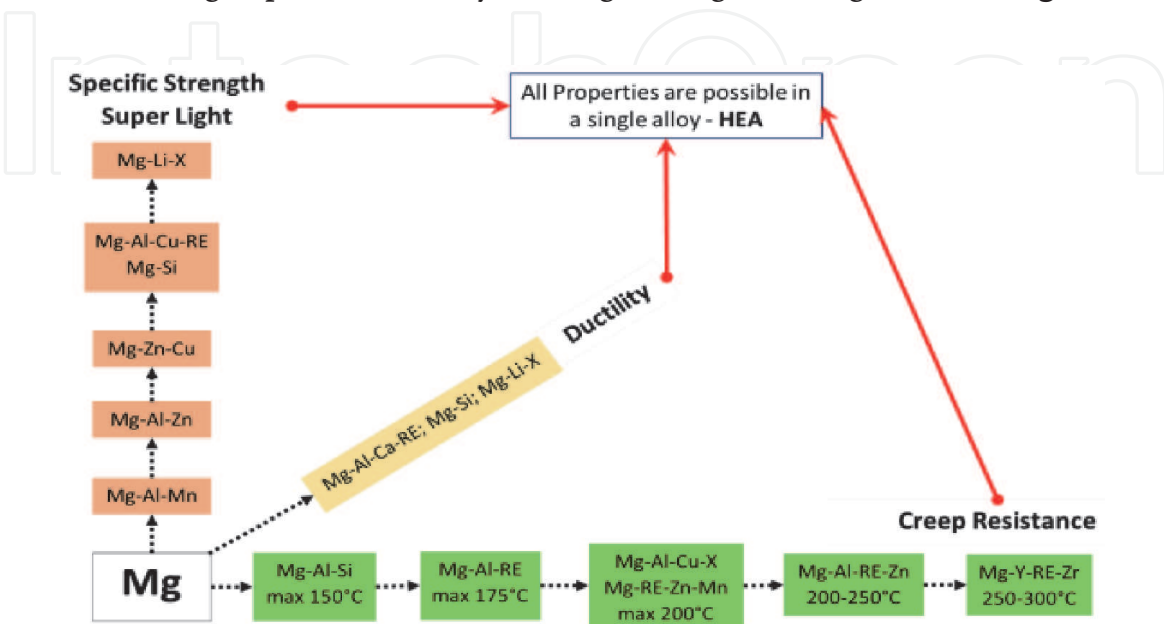


**Figure 2.**
*Development of magnesium alloys.*
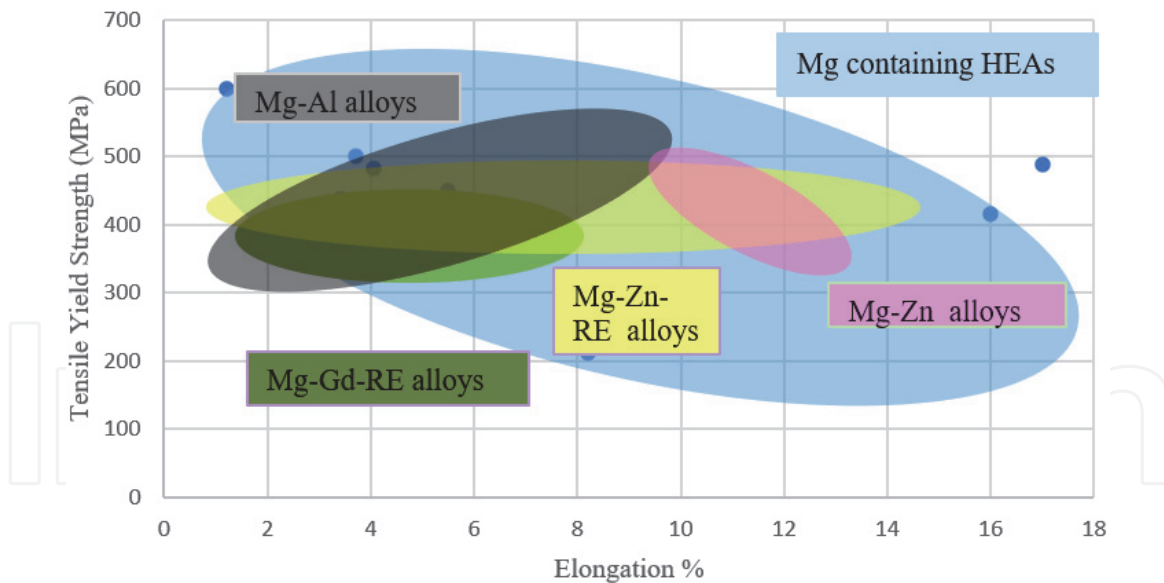
**Figure 3.**
*Tensile yield strength versus elongation %.*

Mg containing HEAs may have property in a combination of all (cocktail effect). Most Mg containing HEAs show light weight and moderate strength which is described in the mechanical properties section 6. A combination of the light weight achieved due to Mg being one of the base metals and the superior properties of the other principal elements makes HEAs special.

**Figure 3** shows graph of tensile yield strength versus elongation of a range of Mg-Al, Mg-Zn, Mg-Zn-RE, Mg-Gd-RE alloys and Mg containing HEAs [30–35]. The available data on Mg containing HEAs are used in this plot and the other Mg alloy range is obtained from a study by Sankaran and coworkers [30]. This diagram shows the wide range of tensile strength and elongation depending on the compositions of alloys, which not only contributes to the materials property but also adds new possible alloys for a wide range of applications.

## 5. Synthesis of Mg HEA

**Figure 4** shows Al is the highest alloyed element with Mg followed by Cu and Li in HEA system. Mg is a reactive metal with a low melting point. It burns with a shiny white light in air. Considering its high vapour pressure, Mechanical Alloying (MA) would be a suitable process compared to melting and casting for synthesis of alloys containing Mg. MA is a common route for synthesis of Mg containing HEAs [33, 36–42]. Youssef et. al [37] and Ornov et. al [43] were the first to study Mg containing HEAs synthesized by MA. Initial results were promising for the future of Mg-HEAs. $AlFeCuCrMg_x$ (x = 0, 0.5, 1, 1.7 mol) was synthesized by MA process to understand the effect of composition of Mg on phases and solid solution formability. It has been found that Mg addition stabilizes BCC structure via dissolution of FCC structure [43]. Cold welding supersedes fracturing in alloys with higher Mg. Lattice distortion was found to increase with Mg % in the alloys [43]. A low density Mg containing HEA with FCC phase transformed to more stable HCP structure on annealing and reported high hardness of 5.8 GPa [37]. Due to continuous cold welding and mechanical impact by the balls the atomic density of the powder increases and hence number of slip systems and ductility increases. So, the milling time must be increased with the increase in Mg composition [43]. Maulik and

Kumar confirmed lattice distortion, which increased with further addition of Mg [43]. Although, for sintered alloys, lattice distortion first increased and then decreased with Mg content [38]. Equiatomic MgAlSiCrFe HEA was synthesized by MA and was found to be stable at moderate temperatures (300-500°C), also Si did not dissolve completely even after 60 hours of milling [44]. In the pioneer works on Mg containing HEAs, a similar phenomenon could be identified that conventional threshold limits of $\Delta H_{mix}$ and $\delta$ do not support the formation of solid solution but there is still formation of SS [6, 7, 35, 43, 45].
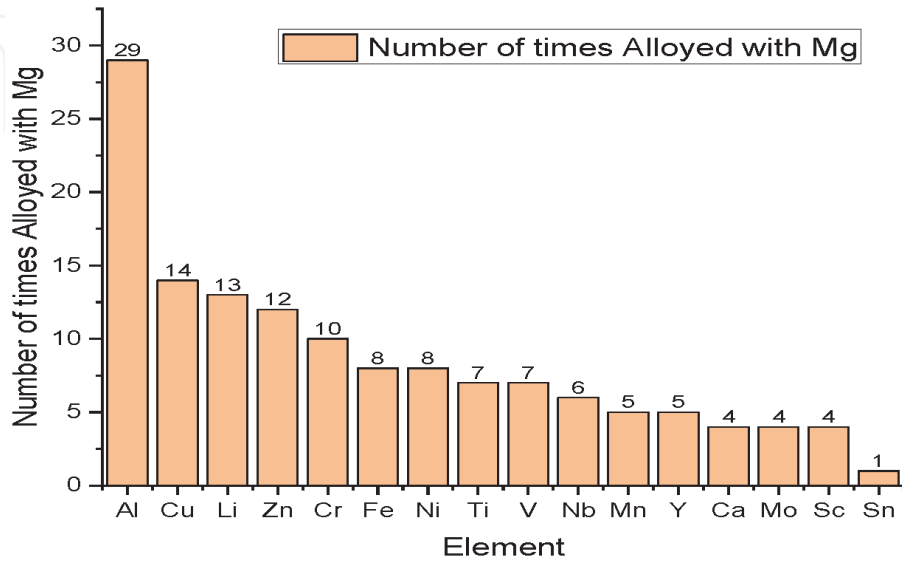


**Figure 4.**
*Elements vs number of times alloyed with Mg.*

| Element | Symbol | Atomic Mass | r (Å) | VEC | X | Density | Tm (K) |
|---|---|---|---|---|---|---|---|
| Lithium | Li | 6.941 | 1.57 | 1 | 0.98 | 0.534 | 453.69 |
| Magnesium | Mg | 24.305 | 1.6 | 2 | 1.31 | 1.738 | 923 |
| Aluminium | Al | 26.9815 | 1.43 | 3 | 1.61 | 2.7 | 933.52 |
| Calcium | Ca | 40.078 | 2 | 2 | 1 | 1.55 | 1123 |
| Scandium | Sc | 44.9559 | 1.6 | 3 | 1.36 | 2.985 | 1812 |
| Titanium | Ti | 47.88 | 1.47 | 4 | 1.54 | 4.506 | 1943 |
| Vanadium | V | 50.9415 | 1.36 | 5 | 1.63 | 6.11 | 2190 |
| Chromium | Cr | 51.996 | 1.28 | 6 | 1.66 | 7.19 | 2130 |
| Manganese | Mn | 54.93805 | 1.12 | 7 | 1.55 | 7.21 | 1517 |
| Iron | Fe | 55.847181 | 1.28 | 8 | 1.83 | 7.874 | 1810 |
| Nickel | Ni | 58.69 | 1.5 | 10 | 1.91 | 8.908 | 1728 |
| Copper | Cu | 63.546 | 1.28 | 11 | 1.9 | 8.96 | 1357.7 |
| Zinc | Zn | 65.39 | 1.37 | 12 | 1.65 | 7.14 | 692.8 |
| Yttrium | Y | 88.9059 | 1.81 | 3 | 1.22 | 4.472 | 1803 |
| Niobium | Nb | 92.9064 | 1.47 | 5 | 1.6 | 8.57 | 2750 |
| Molybdenum | Mo | 65.9064 | 1.4 | 6 | 2.16 | 10.28 | 2883 |
| Tin | Sn | 118.71 | 1.58 | 4 | 1.96 | 7.265 | 505.12 |

**Table 2**
*Physical properties of elements.*

The $\Delta H_{mix}$ values in **Table 2** are taken from [46, 47] in which the values have been calculated using Miedema Model [48–52]. A significant portion of the high entropy alloys are produced using the induction melting route [32, 34, 35]. It can be easily inferred from the **Table 2** that there is unavoidable formation of intermetallic and Al-Mn quasicrystals which is majorly because of high negative values of $\Delta H_{mix}$ for various binary pairs given in **Table 2**.

## 6. Microstructure and mechanical behavior of magnesium containing HEAs

Microstructure of a material has a direct influence on its mechanical behaviors. Equiatomic MgMnAlZnCu HEA produced using induction melting consists of a matrix and a floral pattern where the floral pattern is rich in Al-Mn icosahedral quasicrystals and the matrix consists of an HCP phase comprised of all the alloying elements [31]. The presence of the quasicrystals is responsible for the increased hardness in this alloy, which gradually increases upon increasing the cooling rate. It is worth noting that Al-Mn quasicrystals are thermally stable. The increase in cooling rate also changes the plasticity of the alloy and hence, it increases the elasticity [31]. The microstructures are given in the following **Figure 5(a)**. Increasing the amount of Mg in the alloy reduced the $\Delta H_{mix}$, as a result, there is increase in the amount of SS phases [32]. Along with the HCP and icosahedral quasicrystalline phases, a pure Mg and $Mg_7Zn_3$ phases are present in Magnesium
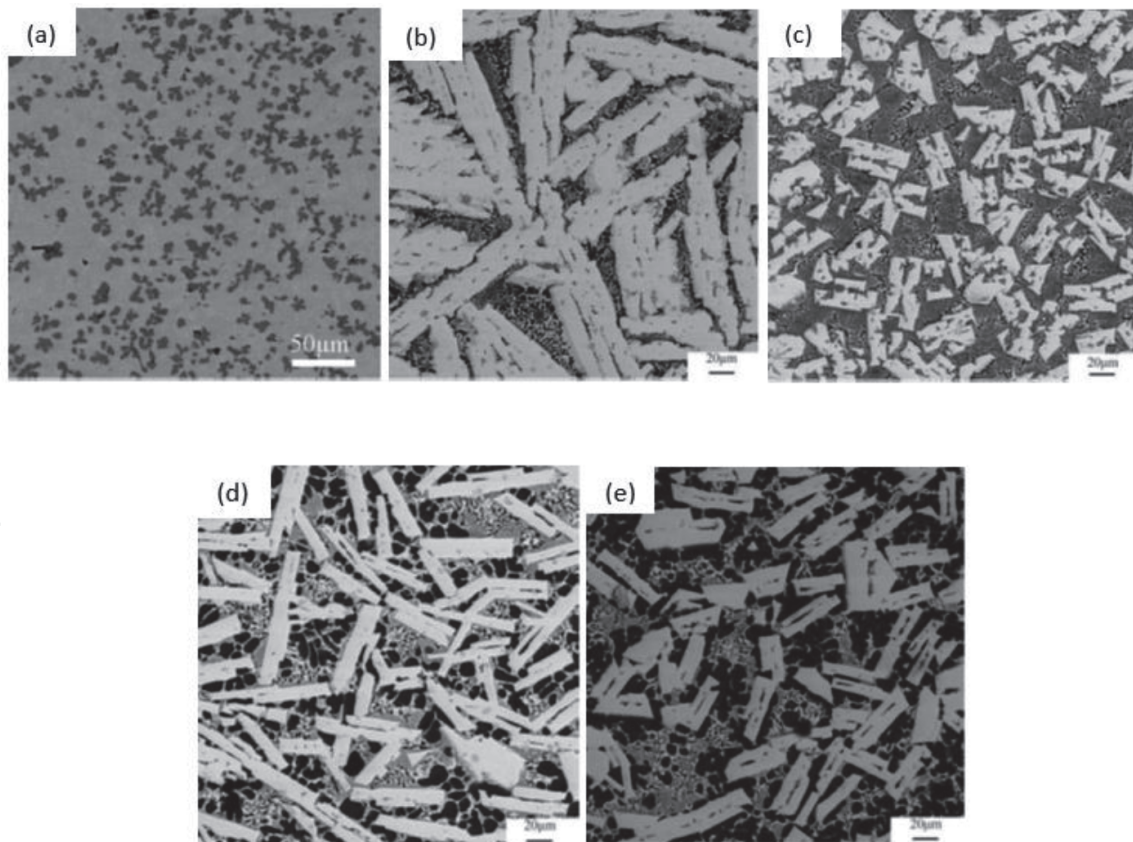


**Figure 5.**
*(a) Equiatomic MgMnAlZnCu (Induction melting in Ar atmosphere, cooled using brine in Cu mold), (b) $Mg_{33}(MnAlZnCu)_{67}$ (Induction melting in Ar atmosphere, Air cooling in Cu mold), (c) $Mg_{43}(MnAlZnCu)_{57}$ (Induction melting in Ar atmosphere, Air cooling in Cu mold), (d) $Mg_{45.6}(MnAlZnCu)_{54.4}$ (Induction melting in Ar atmosphere, Air cooling in Cu mold), (e) $Mg_{50}(MnAlZnCu)_{50}$ (Induction melting in Ar atmosphere, Air cooling in Cu mold) (Reprinted with permission from Refs. [31,32]).*

containing entropy stabilized alloy systems. Increase in Mg content enhances the complexity of the microstructures as per the **Figure 5(b)-(e)** [32].

Another light weight Mg-HEA, $Al_{60}Cu_{10}Fe_{10}Cr_5Mn_5Ni_5Mg_5$, fabricated using vacuum induction melting followed by die casting, exhibits three different phases (1) $Al_3Fe_4$, (2) $Al_7Cu_4Ni$ and (3) $Mg_2Cu_6Al_5$ in the SEM image (**Figure 6.**) [34].

Tun et. al. fabricated $Mg_{80}Al_5Cu_5Mn_5Zn_5$ HEA through disintegrated melt deposition followed by extrusion: The alloy showed two IM and one SS phase in the microstructure [53]. The microstructure contained $Al_6Mg$ and $Al_2CuMg$ intermetallics and an HCP phase containing Mg, Mn and Al. The microstructure of $Mg_{80}Al_5Cu_5Mn_5Zn_5$ HEA is shown in **Figure 7(a)**. Phases mentioned as 1, 2 and, 3 are the HCP phase, $Al_6Mg$ and $Al_2CuMg$ phases respectively.

The density of any high entropy system is highly dependent on the elements present in the alloy. Mg and Li system produces extremely light weight alloys while addition of Al increases density but it strengthens the system as well. This increases the specific strength, which makes magnesium based high and medium entropy systems a matter of interest these days. The highest density in any magnesium containing multi-element alloy system is 5.06 g/cc in equiatomic MgMnAlZnCu produced using induction melting followed by cooling in brine, whereas $Mg_{80}Al_5Cu_5Mn_5Zn_5$ exhibits the lowest density of 2.15 g/cc. The other available density data is given in **Table 3**.

The hardness of Mg-HEAs generally decreased with increase in composition of Mg, the maximum hardness with equiatomic composition was found to be 428 HV [32]. MgMnAlZnCu HEA exhibits the highest hardness when processed at higher cooling rate due to formation of Al-Mn icosahedral quasicrystals [31].

Mg-HEAs with a low magnesium content exhibit higher yield strength. The $Al_{60}Cu_{10}Fe_{10}Cr_5Mn_5Ni_5Mg_5$ exhibits a yield strength of 743 MPa, while magnesium rich systems can result in yield stress as low as 211 MPa. The yield strength data
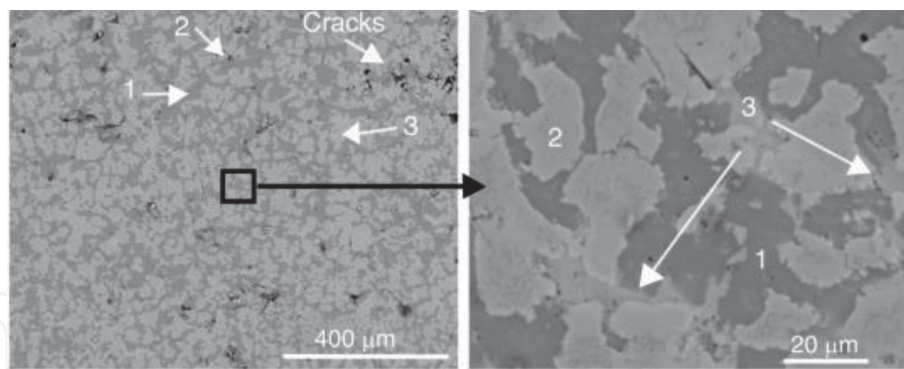


**Figure 6.**
*SEM micrographs of* $Al_{60}Cu_{10}Fe_{10}Cr_5Mn_5Ni_5Mg_5$ *(Reprinted with permission from Ref. [34]).*
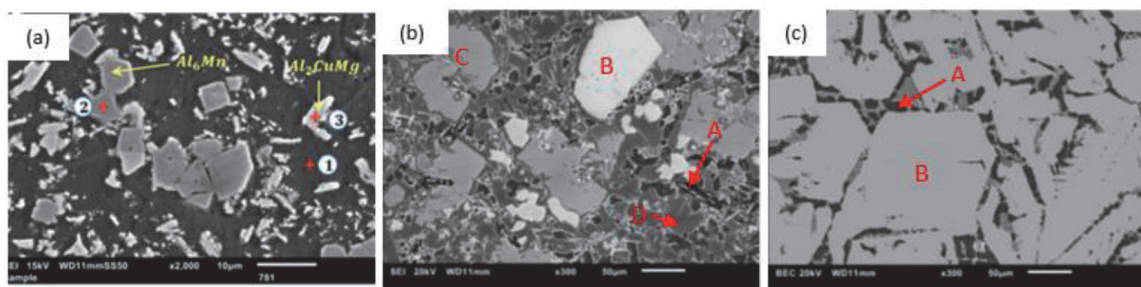


**Figure 7.**
*SEM micrograph of* (a) $Mg_{80}Al_5Cu_5Mn_5Zn_5$ , *(b)* $Mg_{35}Al_{33}Li_{15}Zn_7Ca_5Y_5$ *and (c)* $Mg_{35}Al_{33}Li_{15}Zn_7Ca_5Cu_5$
*(image (a) adapted from Ref. [53], image (b) and (c) Reprinted with permission from Ref. [33]).*

|     | Mg  | Al  | Cu  | Li  | Zn  | Fe  | Ti  | Cr  | Mn  | Nb  | V   | Ni  | Mo  | Sn  | Sc  | Ca  | Y   |
| --- | --- | --- | --- | --- | --- | --- | --- | --- | --- | --- | --- | --- | --- | --- | --- | --- | --- |
| Al  | -2  |     |     |     |     |     |     |     |     |     |     |     |     |     |     |     |     |
| Cu  | -3  | -1  |     |     |     |     |     |     |     |     |     |     |     |     |     |     |     |
| Li  | 0   | -4  | -5  |     |     |     |     |     |     |     |     |     |     |     |     |     |     |     |
| Zn  | -4  | 1   | 1   | -8  |     |     |     |     |     |     |     |     |     |     |     |     |     |     |
| Fe  | 18  | -11 | 13  | 26  | 4   |     |     |     |     |     |     |     |     |     |     |     |     |     |
| Ti  | 16  | -30 | -9  | 34  | -15 | -17 |     |     |     |     |     |     |     |     |     |     |     |     |
| Cr  | 24  | -10 | 12  | 35  | 5   | -1  | -7  |     |     |     |     |     |     |     |     |     |     |     |
| Mn  | 10  | -19 | 4   | 19  | -6  | 0   | -8  | 2   |     |     |     |     |     |     |     |     |     |     |
| Nb  | 32  | -18 | 3   | -46 | -1  | -16 | 2   | -7  | -4  |     |     |     |     |     |     |     |     |     |
| V   | 23  | -16 | 5   | 37  | -2  | -7  | -2  | -2  | -1  | -1  |     |     |     |     |     |     |     |     |
| Ni  | -4  | -22 | 4   | 1   | -9  | -2  | -35 | -7  | -8  | -30 | -18 |     |     |     |     |     |     |     |
| Mo  | 36  | -5  | 19  | 49  | 12  | -2  | -4  | 0   | 5   | -6  | 0   | -7  |     |     |     |     |     |     |
| Sn  | -9  | 4   | 7   | -18 | 1   | 11  | -21 | 10  | -7  | -1  | -1  | -4  | 20  |     |     |     |     |     |
| Sc  | -3  | -38 | -24 | 12  | -29 | -11 | 8   | 1   | -8  | 18  | 7   | -39 | 11  | -45 |     |     |     |     |
| Ca  | -6  | -20 | -13 | -1  | -22 | 25  | 43  | 38  | 19  | 63  | 44  | -7  | 56  | -45 | 17  |     |     |     |
| Y   | -6  | -38 | -22 | 8   | -31 | -1  | 15  | 11  | -1  | 30  | 17  | -31 | 24  | -51 | 1   | 11  |     |     |

**Table 3**
*Enthalpy of mixing of elements in a pair.*

testifies for the brittleness caused due to presence of high amount of Mg. The behavior is predominantly because of HCP structure induced by higher percentage of Mg which inhibits dislocation by insufficient number of slip systems. Although by adding Li with 10.3 wt% in Mg the crystal structure changes from HCP to BCC. The properties of Mg-HEAs are better than conventional Magnesium alloys. The reason behind this lies in the formation of a complex mixture of intermetallics and solid-solution phases in the system according to a study on $Mg_{80}Al_5Cu_5Mn_5Zn_5$ by Tun et. al. [53].

It can be inferred from existing literature, Mg-HEAs synthesized by MA can find applications in structural as well as hydrogen storage systems [39, 41, 54–57] although more extensive research is required to find a better alloy and processing techniques; whereas induction melting in different atmospheres and casting process were used for alloys to be used in load bearing components. Mechanical properties are available for a few alloys which makes it difficult for authors to give a comprehensive analysis. $MgMoNbFeTi_2$ and Y doped $MgMoNbFeTi_2$ were synthesised using mechanical alloying followed by laser cladding. Increase in Yttria content resulted in enhanced mechanical properties of the alloy [36]. It is well established that for enhancement of mechanical properties, Mg alloys are doped with reactive elements like Re, Y and Hf.

**Table 4** represents the manufacturing route for various Mg containing HEAs, the phases present in corresponding alloys, the presence of intermetallic phases and the physical and mechanical properties of the alloys. It is evident from the data that the presence of intermetallics enhance the mechanical properties of the alloys. The increased amount of Mg reduces the alloy density and makes it a suitable candidate for aerospace applications. Further researches on Mg-HEAs need to aim on creating light weight and strong alloys at the same time, this could be done by *thermo-mechanical processing*, which is not yet explored for Mg-HEAs.

| HEA Composition | Processing Route | Phases | | | | Reported Properties | | | | Year | Ref |
|---|---|---|---|---|---|---|---|---|---|---|---|
| | | FCC | BCC | HCP | Intermetallics | Tensile Strength (MPa) | Compressive Strength (MPa) | Hard-ness (HV) | Density (g/cc) | | |
| $Al_{20}Li_{20}Mg_{10}Sc_{20}Ti_{30}$ | Mechanical alloying | | | ✓ | | | | | 3.05 | 2015 | [37] |
| AlLiMgSnZn | Induction Melting | ✓ | | ✓ | ✓ | | 615 | | 3.88 | 2014 | [35] |
| $AlLi_{0.5}MgSc_{0.2}Zn_{0.5}$ | | ✓ | | | ✓ | | 546 | | 2.9 | | |
| $AlCu_{0.2}Li_{0.5}MgZn_{0.5}$ | | | | | ✓ | | | | 2.75 | | |
| $AlCu_{0.5}Li_{0.5}MgSn_{0.2}$ | | | | | ✓ | | | | 2.96 | | |
| $Al_8Li_{0.5}Mg_{0.5}Sn_{0.5}Zn_{0.5}$ | | ✓ | | | ✓ | | 836 | | 3.05 | | |
| $Al_8Cu_{0.5}Li_{0.5}Mg_{0.5}Zn_{0.5}$ | | ✓ | | | ✓ | | 879 | | 2.91 | | |
| $AlFeCuCrMg_{0.5}$ | Mechanical Alloying | | 0.44 | | 0.56 | | | | NA | 2017 | [38] |
| AlFeCuCrMg | | | 0.505 | | 0.495 | | | | NA | | |
| $AlFeCuCrMg_{1.7}$ | | | 0.1 | | 0.9 ($Cu_2Mg$ major) | | | | NA | | |
| $Mg_{20}(MnAlZnCu)_{80}$ | Induction Melting | | | ✓ | Al-Mn quasicrystal | | 428 | 428 | 4.3 | 2010 | [32] |
| $Mg_{33}(MnAlZnCu)_{67}$ | | | | ✓ | Al-Mn quasicrystal | | 437 | 324 | 3.5 | | |
| $Mg_{43}(MnAlZnCu)_{57}$ | | | | ✓ | Al-Mn quasicrystal | | 500 | 244 | 2.5 | | |
| $Mg_{45.6}(MnAlZnCu)_{54.4}$ | | | | ✓ | Al-Mn quasicrystal | | 482 | 223.2 | 2.3 | | |
| $Mg_{50}(MnAlZnCu)_{50}$ | | | | ✓ | Al-Mn quasicrystal | | 400 | 178 | 2.2 | | |
| $Mg_{80}Al_5Cu_5Mn_5Zn_5$ | Disintegrated melt deposition. | | | ✓ | ✓ | 318 | 616 | 196 | 2.15 | 2019 | [53] |
| MgVAlCr | Mechanical Alloying | | ✓ | | | | | | NA | 2021 | [39] |
| MgVAlNi | | | ✓ | | | | | | NA | | |
| MgVCrNi | | | ✓ | | | | | | NA | | |
| MgVAlCrNi | | | ✓ | | | | | | NA | | |
| $Mg_{28}V_{28}Al_{19}Cr_{19}Ni_6$ | | | ✓ | | | | | | NA | | |
| $Mg_{26}V_{31}Al_{31}Cr_6Ni_6$ | | | ✓ | | | | | | NA | | |

| HEA Composition | Processing Route | Phases | | | | Reported Properties | | | | Year | Ref |
|---|---|---|---|---|---|---|---|---|---|---|---|
| | | FCC | BCC | HCP | Intermetallics | Tensile Strength (MPa) | Compressive Strength (MPa) | Hard-ness (HV) | Density (g/cc) | | |
| $Mg_{0.1}Ti_{0.3}V_{0.25}Zr_{0.1}Nb_{0.25}$ | Mechanical Alloying | | ✓ | | | | | | NA | 2021 | [41] |
| $Al_{35}Cr_{14}Mg_6Ti_{33}V_{10}$ | Mechanical Alloying | | ✓ | ✓ | | 1503 | | 460 | 4.91 | 2019 | [42] |
| MgAlSiCrFe | Mechanical Alloying | minor | ✓ | | $Mg_2$ Si (Major) | | | | NA | 2020 | [44] |
| AlMgLiCa | Casting | | | | | | | NA | NA | 2020 | [58] |
| $Al_2MgLiCa$ | | | | | | | | ≈300 | NA | | |
| $AlMgLiCa_{0.3}$ | | | | | | | | NA | NA | | |
| $Al_{60}Cu_{10}Fe_{10}Cr_5Mn_5Ni_5Mg_5$ | Vacuum Induction Melting | ✓ | | | ✓ | | | 743 | NA | 2018 | [34] |
| $MgMoNbFeTi_2$ | Mechnaical Alloying;laser cladding (Coating) | | ✓ | | | | | ≈400 | NA | 2020 | [36] |
| $MgMoNbFeTi_2Y_{0.004}$ | | | ✓ | | | | | ≈500 HV | NA | 2020 | |
| $MgMoNbFeTi_2Y_{0.008}$ | | ✓ | ✓ | | | | | ≈650 | NA | 2020 | |
| $MgMoNbFeTi_2Y_{0.012}$ | | ✓ | ✓ | | | | | ≈1000 | NA | 2020 | |
| $Mg_{35}Al_{33}Li_{15}Zn_7Ca_5Y_5$ | Disintegrated melt deposition | | | α-Mg | ✓ | | | 237 ± 10 | 2.25 | 2018 | [33] |
| $Mg_{35}Al_{33}Li_{15}Zn_7Ca_5Cu_5$ | | | | α-Mg | ✓ | | | 267 ± 15 | 2.27 | 2018 | |

**Table 4.**
*Manufacturing routes, present phases and corresponding mechanical properties of Mg containing HEAs.*

## 7. Computational approach in phase identification of magnesium containing high entropy alloys

A large number of researches have been conducted on binary and ternary alloys but quaternary and quinary systems are yet to be explored. The number of possible HEAs are around $10^{177}$ [59]. In order to screen out alloys for use, Calculation of Phase Diagrams (CALPHAD) is an exceptional tool. CALPHAD can be time consuming compared to Molecular Dynamics (MD) and Density Functional Theory (DFT) simulations. CALPHAD uses the phase diagrams and thermodynamics to determine the phases present in a new alloy. Although there is no database for Mg and Li containing HEAs due to insufficient amount of research published till date. There is need of First-principle DFT; MD simulation and Phase Field modelling to gain a better understanding of phases formation and understanding the factors that affects it.

Sanchez et al. used CALPHAD to predict phases present in $Al_{60}Cu_{10}Fe_{10}Cr_5Mn_5Ni_5Mg_5$ alloy and found the Cu, Mg, Ni doped $Al_3Fe_4$, $Al_7Cu_4Ni$, $Al_8Mn_5$, $D8_{10}$ Al-Cr alloy phase and $Mg_2Cu_6Al_5$ phases in the system [34]. The thermo-calc database successfully detected the phases present. Although, there are few discrepancies between the experimental results and Thermo-Calc calculations. CALPHAD predicted more constituent phases of which only few are reported by experiments. This suggests that despite having a slow cooling rate of solidification, total equilibrium state is not achieved in the manufacturing of the alloys. In general, this database has proven to be a good method for designing such HEAs [34].

## 8. Hydrogen storage behavior of Mg-containing HEAs

Amongst the growing need for energy and constant decline in non-renewable energy sources, renewable energy storage devices are gaining popularity. The demand for Hydrogen Storage Devices is also increasing for the same reason. Among many other alternatives of hydrogen storage principles, metal hydrides are considered as some ideal candidates as these do not require cryogenic cooling like liquid hydrogen storages and can absorb decent amount of hydrogen as hydrides due to the high bond strength between metal and hydrogen [54]. Most metal hydrides exhibit exothermic reactions during hydride formation, whereas; the desorption reaction is endothermic in most cases.. So, external temperature rise is necessary to continue the storage cycle. The negative enthalpy and entropy values are responsible for the high bond strength between metal ions and hydrogen [40]. The $\Delta H$=-74 kJ.$mol_{H_2}^{-1}$ and $\Delta S \sim$-135 J.$K^{-1}mol_{H_2}^{-1}$ for $MgH_2$ [40, 54]. The major drawback of single metal hydrides is the low desorption of hydrogen leading to low cyclability [54]. Single metal hydrides exhibit a hydrogen to metal ratio, [H]/[M]= 0.6. To solve this issue, several approaches have been taken e.g. using two or more metals to form hydrides, using non-hydride compositions for hydrogen storage, using boro-hydrides and ultimately, MPEA, commonly known as HEA which are a matter of research now [54].

The hydrogen storage in HEAs is related to a reversible phase transformation upon hydrogen absorption. The complex crystal structure of HEAs can store hydrogen in both tetrahedral and octahedral voids simultaneously, resulting in a higher hydrogen storage capacity than any single or, binary metal hydride. TiVZrNbHf HEA has the hydrogen to metal ratio, [H]/[M]= 2.5 [57]. The hydrogen to metal ratio is 2 for single metal hydrides [41].

Zepon et. al. conducted a research on Mg containing HEA and found the hydrogen absorption capacity to be 1.2 wt% of the alloy. The HEA exhibits a BCC structure while it converts into an FCC structure upon hydrogen absorption [55]. The HEA was produced using high energy ball milling while the hydride was produced using reactive ball milling. The main reason for upgrading to Mg containing HEAs for hydrogen storage is because of the light weight of Mg which might reduce the weight of hydrogen storage devices in light duty fuel cell vehicles. Efficient hydrogen storage requires light weight storage devices for high gravimetric capacity [41].

Marcelo et. al. produced hydrides of MgVCr and MgVTiCrFe alloys using reactive milling and the MgVCr consisted of a BCC phase with presence of β-$MgH_2$ on 72 hours of reactive milling. While the MgVTiCrFe consisted of amorphous phase in this study. The hydrogen storage capacity was measured at 30°C, 150°C and 350°C temperature. The hydrogen storage capacity was observed to be extremely low at 30°C and 150°C while it increased at 350°C. The MgVTiCrFe alloy did not show very promising hydrogen storage characteristics but MgVCr is a promising candidate for this purpose exhibiting a reversible 0.95 wt% hydrogen absorption capacity [56].

Strozi et. al synthesized MgVAlCrNi HEA using high energy ball milling but the equiatomic compound showed a very low hydrogen storage capacity, so two non-equiatomic alloy, $Mg_{28}V_{28}Al_{19}Cr_{19}Ni_6$ and $Mg_{26}V_{31}Al_{31}Cr_6Ni_6$ were proposed and studied for hydrogen storage which also didn't show promising results. The non-equiatomic compositions were selected in such a way that the amount of Mg and V is increased, the solubility of hydrogen is increased and so does the lattice parameter because, the increase in lattice parameter indicates that there will be more available interstitial space for hydrogen absorption into the structure. This study prioritizes on the importance of the enthalpy of hydrogen solution on the hydrogen storage capacity of Mg containing HEAs [39]. The positive enthalpy of hydride formation for most of the elements present in these alloys is responsible for this low hydrogen storage behavior.

A very recent study by Montero et al. suggests the improvement in cycling behavior of TiVZrNb HEA upon introduction of Mg to it. After the 12th cycle, the absorption capacity reduces upto 2.41 wt% from the initial 2.8 wt%. The temperature where the maximum desorption occur, is 290°C for $Mg_{10}Ti_{10}V_{25}Zr_{10}Nb_{25}$, while it is 330°C for $Ti_{32.5}V_{27.5}Zr_{12.5}Nb_{27.5}$ [41]. As the desorption reaction is endothermic, it requires external temperature rise to promote the process. The lower the temperature when the desorption starts, the more economically viable and efficient the storage device will be. This particular composition shows the lowest temperature for the maximum desorption to occur. Observations from this study suggests that the $Mg_{10}Ti_{10}V_{25}Zr_{10}Nb_{25}$, alloy loses around 11 % of the hydrogen storage capacity in the second cycle, where the storage capacity reduces from 2.7% to

| HEA composition | Hydrogen absorption capacity | Desorption temperature | [H]/[M] | Ref. |
|---|---|---|---|---|
| $MgZrTiFe_{0.5}Co_{0.5}Ni_{0.5}$ | 1.2 wt% | 300°C | 0.7 | [55] |
| MgVCr | 0.95 wt% | 376°C | | [56] |
| MgVTiCrFe | 0.37 wt% | 360°C | | [56] |
| MgVAlCrNi | 0.3 wt% | 440°C | ~0.15 | [39] |
| $Mg_{10}Ti_{10}V_{25}Zr_{10}Nb_{25}$ | 2.8 wt% | 290°C | 1.7 | [41] |

**Table 5.**
*Hydrogen absorption capacity of HEAs.*

2.41%, whereas, $Ti_{32.5}V_{27.5}Zr_{12.5}Nb_{27.5}$ loses 28% of the hydrogen storage capacity during the first 4 cycles. This recent study suggests the enhancement in the reversable capacity of Mg containing HEAs than Mg-less HEAs. There are not many studies done on Mg containing HEAs for hydrogen storage applications and so the field is open for further research. But this particular study suggests a high potential of Mg containing MPEAs in this certain application.

The **Table 5** summarizes the findings.

## 9. Design, phase prediction and future of Mg HEA

This section gives an elementary guideline for design, phase prediction and future trends of magnesium containing HEAs. Before doing that it is more important to focus on possible applications of such alloys e.g. die casting, paneling of aircraft, weight reduction in automobiles and biomedical implants. Magnesium components are used in automobiles as instrument-panel beam, transfer case, steering components, air bag housing, seat tanks, fuel tank cover and radiator support. Typically Mg constitutes 4 kgs of normal cars weight which is fairly less. Mg can absorb 16 time more vibrations compared to Al, hence alloys of Mg can be used for shock absorbing applications. The major reason for limited use of Magnesium alloys is low strength compared to Aluminum alloys and Steels. The concept of maximization of entropy via mixing multiple elements in near equiatomic ratios to creating "base" or solvent less alloy. Till date, various HEAs have proven their strength. The implementation of this system to Mg could be breakthrough for automotive, space, missiles and aircraft industry. To do so authors provide a preliminary scientific approach to develop Mg HEAs.

Mg has high solubility with Li ($\sim$ 17 at. %), Al ($\sim$12 at. %), In ($\sim$19 at. %) and it is completely soluble with Cadmium. Although Li and In are soft metals like Mg. It has very high tendency to form intermetallic compounds with metals such as Al, Zn, Cu, Y, Zr and Ca etc. It forms the famous quasicrystals when alloyed with Mn. Mg finds place in a wide spectrum of alloys, compounds and systems. Perhaps it is most interesting element, yet to be studied thoroughly in the complex concentrated systems or HEAs. The short range order in HEAs is recently reported to be a core effect for strengthening in such alloys. Mg provides a great avenue for tailoring heterogeneities in HEAs. In the light of limited data of Mg containing HEAs with only 35 compositions, it is hard for authors to suggest the role of thermodynamic and kinetic criteria to develop Mg-HEAs. There is an insufficient data to develop an analogy on the phase development and phase evolution of Mg containing HEAs.

It has been understood that critical values of theoretical parameters used for conventional heavy HEAs are not sufficient and effective in case of LHEAs containing especially Mg owing to its larger size, high |ΔHmix| with most of elements leading to immiscibility (ΔHmix is +ve) and intermetallic formation (ΔHmix is –ve). Yang et. al. proposed new limits to the critical value for light weight HEAs. The modified threshold values suggest that SS will form at ΔHmix ∈ [-1, 5] kJ/mol; δ < 4.5% and Ω > 10. Mg amongst all the elements in the reported alloys has higher radius due to which poly-disparity constant "δ" value is higher and hence does not support complete SS formation. It is evident that Ω > 10 is an ideal condition for SS formation but in various cases a pure SS is obtained when Ω < 10, which is an unknown at present and shall be governed by the effect of individual elements for instance; in few of such alloys Mg was alloyed with refractory elements such as Mo and Nb and in this case, δ had a high value. In few alloys the effect of high configurational entropy of mixing is overshadowed by high negative enthalpy of mixing and high atomic mismatch. HEAs containing Mg, Li and Al open a new

avenue for scientific research and new outlook for understanding of such complex systems. It is simply understood that if an alloy contain more elements with HCP crystal structure (Mg, Ti, Sc, Co, Zn, Cd, Zr and Y), it should probably result in HCP structure of alloy. This is evident from the authors analysis. It can be concluded that for designing HEAs with Mg, Li and Al, ΔHmix should be given priority over entropy of mixing. It is crucial to study the possible binary and ternary combinations out of the sought HEA composition.

For the design of LHEAs, Mg alone should not be essentially alloyed with Al and/or Li. At the same time elements soluble with Al or Li can be used to further increase the disordered structure. As it has been also observed that the presence of d orbital element is necessary to obtain high entropy effect in the alloy [35]. To understand the phases, pseudo binary phase diagrams can also be produced using Thermo-Calc, molecular dynamics simulations or extrapolating the experimental data. Due to lack of experimental data, the extrapolation may not be accurate. Phase formation and phase stabilization can be understood by studying the thermodynamic parameters. Few graphs have been plotted shown in **Figures 8-10** using the basic thermodynamic parameters such as $\Delta H_{mix}, \Delta S_{mix}, \delta, \chi, \Omega$ and VEC from the data shown in **Table 4**, which are considered as the phase formation parameters. Values of these parameters can be calculated from the equations given in the **Table 6** below.

**Table 7** shows the type of compound formation based on the values of $\Delta H_{mix}$ *and* $\Delta S_{mix}$. Larger negative values of mixing enthalpy may lead to the compound formation. For solid solution formation, higher negative values of entropy is required. Positive values of mixing enthalpy and mixing entropy may lead to the elemental or compound segregation within alloys.

**Figure 8** shows the graph between the $\Delta H_{mix}$ and $\frac{\Delta S_{mix}}{R}$, where R is the Gas constant of the data shown in **Table 5**. Graph shows that pure solid solution is stable at entropy higher than 1.13 kJ/mol. IM are observed in both low entropies and higher entropy region as well. Pure solid solution is observed at medium negative values of $\Delta H_{mix}$. One exceptional is when solid solution has been obtained at higher
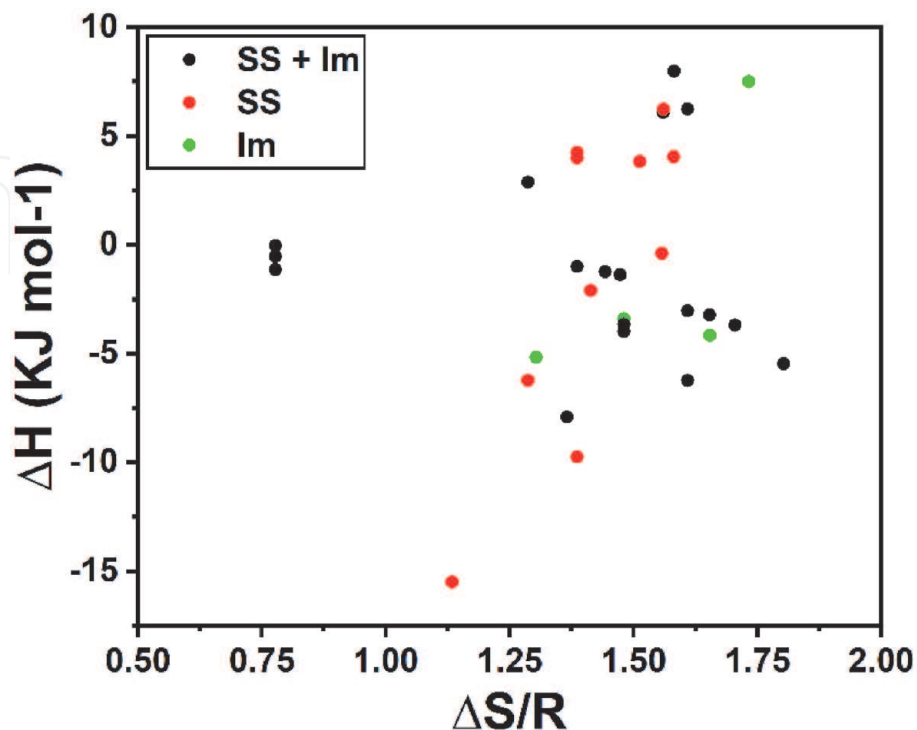


**Figure 8.**
*Graph between enthalpy and entropy from the data shown in **Table 4**.*
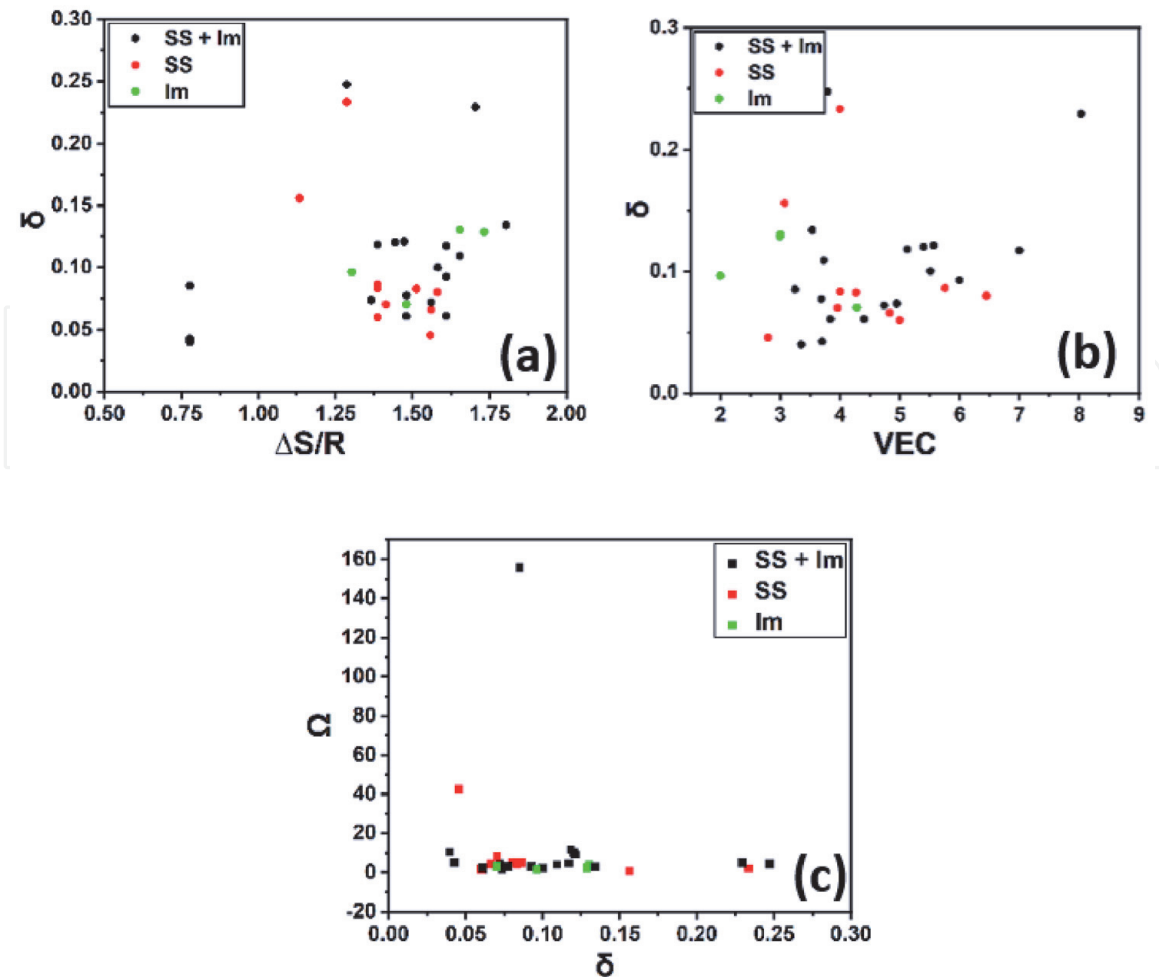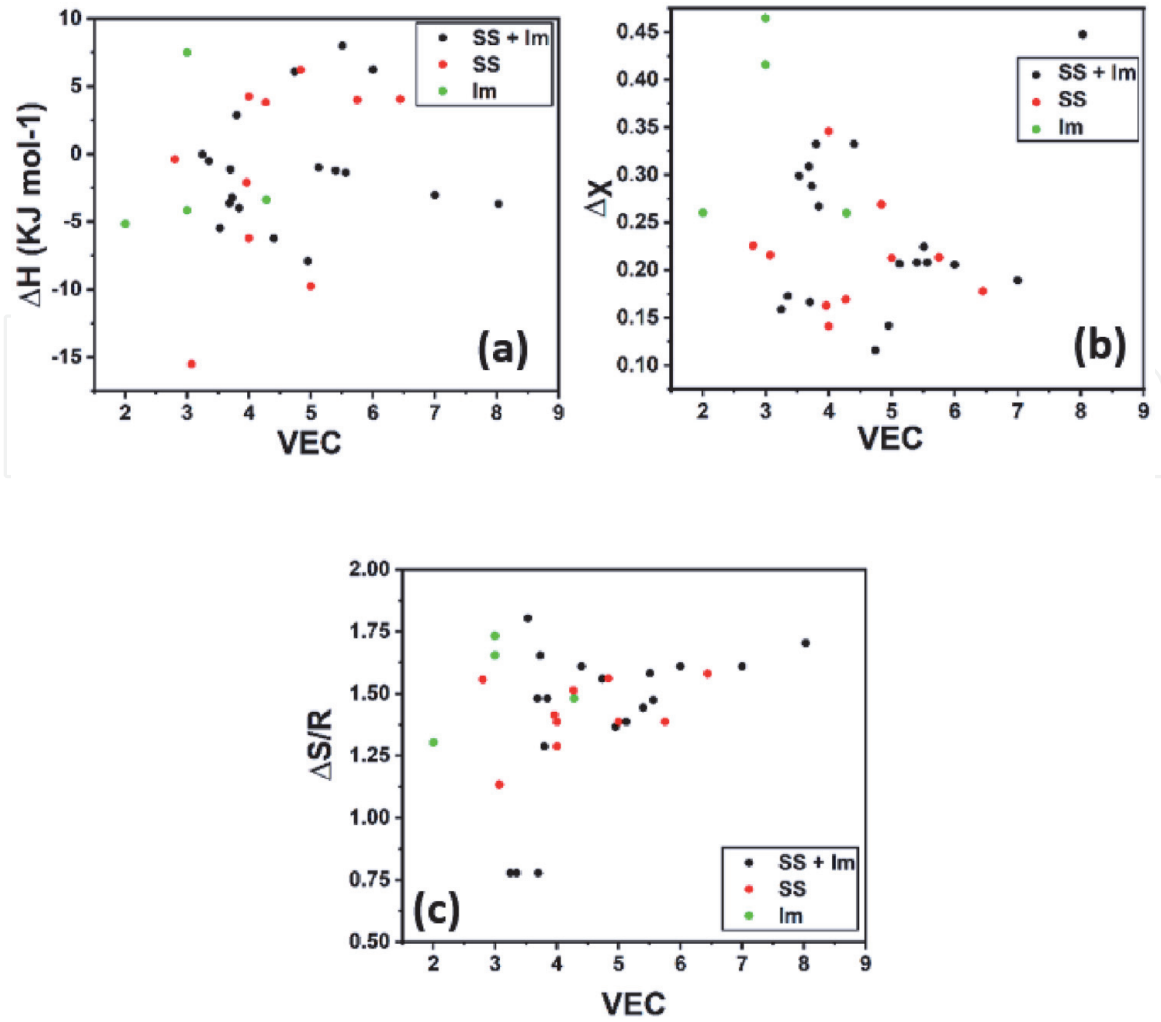
**Figure 9.**
*(a) Graph between atomic mismatch factor and VEC; (b) graph between the atomic mismatch factor and omega; (c) graph between atomic mismatch factor and VEC. Data has been taken from **Table 5**.*

negative value of $\Delta H_{mix}$. That is due to the presence of Ca in the alloy. Mg tends to form stable compounds with the Ca: Presence of Ca enhances the solid solution formation in the presence of Mg.

Effect of $\delta$ is need to be understood properly. As per the Hume Rothery solid solution guidelines, the atomic mismatch factor must be minimum ($\delta \leq 15\%$). The atomic size of light weight elements, Al, Mg, In, Li, Ca is higher as compared to the d block and other elements, due to which there is higher tendency of phase separation. **Figure 9a-c** shows effect of $\delta$ in solid solution formation. The data is used from **Table 5** to plot the graphs against $\frac{\Delta S_{mix}}{R}$ and VEC. **Figure 9a** shows that the pure solid solution are observed only between $0.043 \leq \delta \leq 0.24$. Pure intermetallic compounds are observed between $0.067 \leq \delta \leq 0.133$, and combination of intermetallic and solid solution is observed for rest of the regions as solid solutions are stable only at higher values of entropy, and medium atomic mismatch factor.

**Figure 9b** shows the effect of $\delta$ with the $\Omega$; Ideally, for solid solution formation the value of $\Omega$ should be near 1.1 [60], but solid solutions are also observed at higher values. **Figure 9b** shows that solid solution forms within $0.41 \leq \delta \leq 0.24$ and intermetallic compounds are observed at medium values of $0.066 \leq \delta \leq 0.133$. Combination of solid solution and intermetallic compounds are observed between $0.037 \leq \delta \leq 0.25$. Similarly **Figure 9c** shows that solid solutions are stable between $0.043 \leq \delta \leq 0.24$, longer range of atomic mismatch factor, and intermetallic compounds are observed between $0.067 \leq \delta \leq 0.13$. Combination of solid solution and intermetallic compound is observed at all other regions. These graphs show that

**Figure 10.**
*(a) Graph between VEC and enthalpy; (b) graph between VEC and electro-negativity; (c) graph between VEC and entropy. Data has been taken from **Table 5**.*

| | | | |
|---|---|---|---|
| 1. | Atomic size 2difference | $\delta = \sqrt{\left(\Sigma_i^n c_i \left(1 - \frac{r_i}{\bar{r}}\right)^2\right)}$ <br> $C_i$ is atomic percentage | [35] |
| 2. | Enthalpy | $\Delta H_{mix} = \Sigma_{i=1, i\neq j}^n \Omega_{ij} C_i C_j$ <br> $C_i$ and $C_j$ is atomic percentage | [35] |
| 3. | Macro states: Statistical Thermodynamic parameter | $\Omega = \frac{T_m \Delta S_{mix}}{|\Delta H_{mix}|}$ <br> $T_m$ is the melting point of n elements. | [35] |
| 4. | Melting point of n elements | $T_m = \Sigma_{i=1}^n n_{C_i}(T_m)_i$ <br> n is the number of elements. $C_I$ is the atomic percentage; <br> $T_{mi}$ is the melting point of ith element. | [35] |
| 5. | Pauling electronegativity difference | $\Delta \chi = \sqrt{\Sigma_{i=1}^n c_i(\chi_i - \bar{\chi})^2}$ <br> $C_i$ is the atomic percentage of ith element. <br> $\bar{\chi}$ is average electronegativity <br> $\chi$ is the electronegativity of ith element | [35] |
| 6. | VEC | $VEC = \Sigma_{i=1}^n c_i(VEC)_i$ <br> $C_i$ is the atomic percentage of ith element. | [35] |

**Table 6.**
*List of equations for calculation of thermodynamic parameters.*

| Mixing Enthalpy | Mixing Entropy | Gibbs Free Energy | Types of phase |
|---|---|---|---|
| $\Delta H_{mix} = 0$ | $\Delta S_{mix} = 0$ | $\Delta G_{mix} = 0$ | Elemental Phases |
| $\Delta H_{mix} \ll 0$ *(Large negative)* | $\Delta S_{mix} = 0$ | $\Delta G_{mix} \ll 0$ *(Large negative)* | Compounds |
| $\Delta H_{mix} < 0$ | $\Delta S_{mix} < 0$ *(medium negative)* | $\Delta G_{mix} \ll 0$ *(Large negative)* | Intermediate phase |
| $\Delta H_{mix} < 0$ *(medium negative)* | $\Delta S_{mix} < -1.5R$ | $\Delta G_{mix} \ll 0$ *(Large negative)* | Random solid solution |

**Table 7.**
*Types of phase based on the values of thermodynamic parameters, Gibbs free energy ΔG_mix, mixing enthalpy ΔH_mix and mixing Entropy ΔS_mix [60].*

there is high possibility of ordering within a high entropy solid solution, as also said above [35]. Simple solid solution of HEA could be obtained between $0.041 \leq \delta \leq 0.24$. Solid solution formation is also depending on the values of Valence Electron Concentration (VEC), which are being discussed in section 10.

**Figure 10** shows the effect of VEC on solid solution formation in LHEAs. VEC is the total number of free electrons including the d-orbital electrons that can participate in the formation of chemical bond. Generally, VEC also helps to understand the type of phase formation in the alloy. FCC phases are found to be stable at VEC 8, and BCC phases are stable at VEC<6.87. Combination of BCC + FCC are stable for the value of VEC between 6.87 < VEC < 8.

**Figures 9b** and **10a-c**, shows the effect of VEC on solid solution formation with respect to $\Delta H_{mix}, \chi$ and $\frac{\Delta S_{mix}}{R}$. All of the three graphs shows exact same values for solid solution, Intermetallic compound and combination of solid solution and intermetallic compound formation. Solid solution is observed between 2.7< VEC<6.5; Intermetallic compounds are observed between 1.92<VEC<4.35 and combination of solid solution and intermetallic compounds are observed between 2.8<VEC<8.1.

All the parameters can be understood as the pure ss of LHEA will form for the following parameters.

1. $-15 < \Delta H_{mix} < 6.5$

2. $1.1 < \frac{\Delta S_{mix}}{R} < 1.6$

3. $0.041 \leq \delta \leq 0.24$

4. $2.7 < VEC < 6.5$

If an alloy follows these certain condition, we can obtain the single phase LHEAs.

It is observed that alloys with Ca have a higher tendency to form IM, similar result have been observed by Nagase et. al. The melting point (MP) of constituting elements also plays a significant role, as a higher difference in MP leads to segregation upon cooling. It should also be accepted that formation of IM cannot avoided in Complex concentrated systems as there is always a possibility of two random elements having higher negative enthalpy of mixing. It is important to note that till date no Mg containing HEA has shown LPSO. LPSO containing Mg alloys if possible could have exhibited better properties and stability. VEC rule is well-

established in HEAs, but its drawback is that it does not discuss about lattice other than BCC and FCC, in the case of Mg HEAs, most of the lower density alloys crystallizes in HCP.

## 10. Applications

The unique compositions of HEAs give rise to a new set of properties which makes every high entropy alloy unique. Mg containing high entropy alloys have shown promising features which make them unique for the following applications.

1. Aerospace alloys and alloys in motor vehicles as a replacement of Al based alloys: Aluminium is already a popular materials for construction of motor vehicles and even aerospace materials. Mg being lighter than Al in fact acts as a means of reducing the density of the alloy even more.

2. High strength and corrosion resistant applications.

3. Hydrogen storage devices: The details of the hydrogen storage behaviour of Mg containing HEAs are already discussed in section 6. According to **Table 6**, $MgZrTiFe_{0.5}Co_{0.5}Ni_{0.5}$ and $Mg_{10}Ti_{10}V_{25}Zr_{10}Nb_{25}$ are the most promising candidates for this purpose.

## Conflict of interest

The authors declare no conflict of interest.

## Author details

Prince Sharma[1]*, Nushrat Naushin[2], Sahil Rohila[3] and Abhishek Tiwari[1]

1 Department of Metallurgical and Materials Engineering, Indian Institute of Technology, Kharagpur, WB, India

2 Department of Materials Science and Engineering, Khulna University of Engineering and Technology, Khulna, Bangladesh

3 Department of Materials Science and Metallurgical Engineering, Indian Institute of Technology, Sangareddy, Telangana, India

*Address all correspondence to: princesharma@alumni.iith.ac.in

IntechOpen

## References

[1] G.R. Josyer, Maharshi Bharadwaaj's "The Vymanika Shastra," English Tr, Internaitonal Academy of Sanskrit Research, Mysore-4. eastward ones opened., Mysore, 1973.

[2] B. Ravi, Investment Casting Development: Ancient and Modern Approaches, n.d.

[3] B. Cantor, I.T.H. Chang, P. Knight, A.J.B. Vincent, Microstructural development in equiatomic multicomponent alloys, Mater. Sci. Eng. A. 375–377 (2004) 213–218. https://doi.org/10.1016/j.msea.2003.10.257.

[4] J.-W. Yeh, S.-K. Chen, S.-J. Lin, J.-Y. Gan, T.-S. Chin, T.-T. Shun, C.-H. Tsau, S.-Y. Chang, Nanostructured High-Entropy Alloys with Multiple Principal Elements: Novel Alloy Design Concepts and Outcomes, Adv. Eng. Mater. 6 (2004) 299–303. https://doi.org/10.1002/adem.200300567.

[5] D.B. Miracle, O.N. Senkov, A critical review of high entropy alloys and related concepts, Acta Mater. 122 (2017) 448–511.

[6] P. Sharma, Electro-spark Coating of High Entropy Alloy on Steel and Inconel Superalloy for Surface Hardening and Oxidation Protection, Master Thesis, Indian Institute of Technology Hyderabad 2020. https://doi.org/10.13140/RG.2.2.13942.32327/1.

[7] X. Yang, Y. Zhang, Prediction of high-entropy stabilized solid-solution in multi-component alloys, Mater. Chem. Phys. 132 (2012) 233–238. https://doi.org/10.1016/j.matchemphys.2011.11.021.

[8] J. Dąbrowa, M. Zajusz, W. Kucza, G. Cieślak, K. Berent, T. Czeppe, T. Kulik, M. Danielewski, Demystifying the sluggish diffusion effect in high entropy alloys, J. Alloys Compd. 783 (2019) 193–207.

[9] S. V Divinski, A. V Pokoev, N. Esakkiraja, A. Paul, A mystery of "sluggish diffusion" in high-entropy alloys: the truth or a myth?, in: Diffus. Found., Trans Tech Publ, 2018: pp. 69–104.

[10] K. Kulkarni, G.P.S. Chauhan, Investigations of quaternary interdiffusion in a constituent system of high entropy alloys, AIP Adv. 5 (2015) 97162.

[11] K.-Y. Tsai, M.-H. Tsai, J.-W. Yeh, Sluggish diffusion in Co–Cr–Fe–Mn–Ni high-entropy alloys, Acta Mater. 61 (2013) 4887–4897.

[12] K. Jin, C. Zhang, F. Zhang, H. Bei, Influence of compositional complexity on interdiffusion in Ni-containing concentrated solid-solution alloys, Mater. Res. Lett. 6 (2018) 293–299.

[13] M. Vaidya, S. Trubel, B.S. Murty, G. Wilde, S. V Divinski, Ni tracer diffusion in CoCrFeNi and CoCrFeMnNi high entropy alloys, J. Alloys Compd. 688 (2016) 994–1001.

[14] M. Vaidya, K.G. Pradeep, B.S. Murty, G. Wilde, S. V Divinski, Radioactive isotopes reveal a non sluggish kinetics of grain boundary diffusion in high entropy alloys, Sci. Rep. 7 (2017) 1–11.

[15] M. Vaidya, K.G. Pradeep, B.S. Murty, G. Wilde, S. V Divinski, Bulk tracer diffusion in CoCrFeNi and CoCrFeMnNi high entropy alloys, Acta Mater. 146 (2018) 211–224.

[16] D. Gaertner, J. Kottke, G. Wilde, S. V Divinski, Y. Chumlyakov, Tracer diffusion in single crystalline CoCrFeNi and CoCrFeMnNi high entropy alloys, J. Mater. Res. 33 (2018) 3184–3191.

[17] J. Zhang, G.M. Muralikrishna, A. Asabre, Y. Kalchev, B. Butz, J. Müller, S.

Hilke, H. Rösner, G. Laplanche, S. V Divinski, Tracer Diffusion in the Σ-Phase of the CrMnFeCoNi System, Available SSRN 3688786. (n.d.).

[18] J. Dąbrowa, W. Kucza, G. Cieślak, T. Kulik, M. Danielewski, J.W. Yeh, Interdiffusion in the FCC-structured Al-Co-Cr-Fe-Ni high entropy alloys: Experimental studies and numerical simulations, J. Alloys Compd. 674 (2016) 455–462. https://doi.org/10.1016/j.jallcom.2016.03.046.

[19] V.M. Nadutov, V.F. Mazanko, S.Y. Makarenko, Tracer Diffusion of Cobalt in High-Entropy Alloys AlxFeNiCoCuCr, Металлофизика и Новейшие Технологии. (2017).

[20] S. Ranganathan, Alloyed pleasures: Multimetallic cocktails, Curr. Sci. 85 (2003) 1404–1406.

[21] R.S. Mishra, R.S. Haridas, P. Agrawal, High entropy alloys – Tunability of deformation mechanisms through integration of compositional and microstructural domains, Mater. Sci. Eng. A. 812 (2021) 141085. https://doi.org/https://doi.org/10.1016/j.msea.2021.141085.

[22] F.X. Zhang, S. Zhao, K. Jin, H. Xue, G. Velisa, H. Bei, R. Huang, J.Y.P. Ko, D. C. Pagan, J.C. Neuefeind, W.J. Weber, Y. Zhang, Local Structure and Short-Range Order in a NiCoCr Solid Solution Alloy, Phys. Rev. Lett. 118 (2017) 205501. https://doi.org/10.1103/PhysRevLett.118.205501.

[23] R. Zhang, S. Zhao, J. Ding, Y. Chong, T. Jia, C. Ophus, M. Asta, R.O. Ritchie, A.M. Minor, Short-range order and its impact on the CrCoNi medium-entropy alloy, Nature. 581 (2020) 283–287. https://doi.org/10.1038/s41586-020-2275-z.

[24] M.M. Nygård, W.A. Sławiński, G. Ek, M.H. Sørby, M. Sahlberg, D.A. Keen, B.C. Hauback, Local order in high-entropy alloys and associated deuterides–a total scattering and Reverse Monte Carlo study, Acta Mater. 199 (2020) 504–513.

[25] O. Maulik, D. Kumar, S. Kumar, S.K. Dewangan, V. Kumar, Structure and properties of lightweight high entropy alloys: A brief review, Mater. Res. Express. 5 (2018) 52001. https://doi.org/10.1088/2053-1591/aabbca.

[26] E. Abe, Fascinating LPSO-Structured Mg Alloys, in: Magnes. Technol. 2016, Springer International Publishing, 2016: pp. 11–12. https://doi.org/10.1007/978-3-319-48114-2_4.

[27] L.W. Cheah, Cars on a Diet: The Material and Energy Impacts of Passenger Vehicle Weight Reduction in the U.S, 2001.

[28] M. Gupta, N.M.L. Sharon, Magnesium, Magnesium Alloys, and Magnesium Composites, Wiley, 2011. https://doi.org/10.1002/9780470905098.

[29] M. Mezbahul-Islam, A. Mostafa, M. Medraj, Essential magnesium alloys binary phase diagrams and their thermochemical data, J. Mater. 2014 (2014).

[30] K.K. Sankaran, R.S. Mishra, Chapter 7 - Magnesium Alloys, in: K.K. Sankaran, R.S. Mishra (Eds.), Metall. Des. Alloy. with Hierarchical Microstruct., Elsevier, 2017: pp. 345–383. https://doi.org/10.1016/B978-0-12-812068-2.00007-2.

[31] R. Li, J.C. Gao, K. Fan, Microstructure and mechanical properties of MgMnAlZnCu high entropy alloy cooling in three conditions, in: Mater. Sci. Forum, Trans Tech Publ, 2011: pp. 235–241.

[32] R. Li, J.C. Gao, K. Fan, Study to microstructure and mechanical properties of Mg containing high entropy alloys, in: Mater. Sci. Forum, Trans Tech Publ, 2010: pp. 265–271.

[33] K.S. Tun, M. Gupta, Microstructural evolution in MgAlLiZnCaY and MgAlLiZnCaCu multicomponent high entropy alloys, in: Mater. Sci. Forum, Trans Tech Publications Ltd, 2018: pp. 183–187. https://doi.org/10.4028/www.scientific.net/MSF.928.183.

[34] J.M. Sanchez, I. Vicario, J. Albizuri, T. Guraya, J.C. Garcia, Phase prediction, microstructure and high hardness of novel light-weight high entropy alloys, J. Mater. Res. Technol. 8 (2019) 795–803.

[35] X. Yang, S.Y. Chen, J.D. Cotton, Y. Zhang, Phase Stability of Low-Density, Multiprincipal Component Alloys Containing Aluminum, Magnesium, and Lithium, Jom. 66 (2014) 2009–2020. https://doi.org/10.1007/s11837-014-1059-z.

[36] Z. Gu, P. Mao, Y. Gou, Y. Chao, S. Xi, Microstructure and properties of MgMoNbFeTi2Yx high entropy alloy coatings by laser cladding, Surf. Coatings Technol. 402 (2020) 126303. https://doi.org/10.1016/j.surfcoat.2020.126303.

[37] K.M. Youssef, A.J. Zaddach, C. Niu, D.L. Irving, C.C. Koch, A novel low-density, high-hardness, high-entropy alloy with close-packed single-phase nanocrystalline structures, Mater. Res. Lett. 3 (2014) 95–99. https://doi.org/10.1080/21663831.2014.985855.

[38] O. Maulik, N. Patra, D. Bhattacharyya, S.N. Jha, V. Kumar, Local atomic structure investigation of AlFeCuCrMgx (0.5, 1, 1.7) high entropy alloys: X-ray absorption spectroscopy study, Solid State Commun. 252 (2017) 73–77. https://doi.org/10.1016/j.ssc.2017.01.018.

[39] R.B. Strozi, D.R. Leiva, J. Huot, W.J. Botta, G. Zepon, Synthesis and hydrogen storage behavior of Mg–V–Al–Cr–Ni high entropy alloys, Int. J. Hydrogen Energy. 46 (2021) 2351–2361.

[40] I.P. Jain, C. Lal, A. Jain, Hydrogen storage in Mg: A most promising material, Int. J. Hydrogen Energy. 35 (2010) 5133–5144. https://doi.org/10.1016/j.ijhydene.2009.08.088.

[41] J. Montero, G. Ek, M. Sahlberg, C. Zlotea, Improving the hydrogen cycling properties by Mg addition in Ti-V-Zr-Nb refractory high entropy alloy, Scr. Mater. 194 (2021) 113699.

[42] P. Chauhan, S. Yebaji, V.N. Nadakuduru, T. Shanmugasundaram, Development of a novel light weight Al35Cr14Mg6Ti35V10 high entropy alloy using mechanical alloying and spark plasma sintering, J. Alloys Compd. 820 (2020) 153367.

[43] O. Maulik, V. Kumar, Synthesis of AlFeCuCrMgx (x = 0, 0.5, 1, 1.7) alloy powders by mechanical alloying, Mater. Charact. 110 (2015) 116–125. https://doi.org/10.1016/j.matchar.2015.10.025.

[44] N. Singh, Y. Shadangi, N.K. Mukhopadhyay, Phase Evolution and Thermal Stability of Low-Density MgAlSiCrFe High-Entropy Alloy Processed Through Mechanical Alloying, Trans. Indian Inst. Met. 73 (2020) 2377–2386. https://doi.org/10.1007/s12666-020-02039-y.

[45] Y. Zhang, Y.J. Zhou, J.P. Lin, G.L. Chen, P.K. Liaw, Solid-Solution Phase Formation Rules for Multi-component Alloys, Adv. Eng. Mater. 10 (2008) 534–538. https://doi.org/10.1002/adem.200700240.

[46] A. Takeuchi, A. Inoue, Calculations of Mixing Enthalpy and Mismatch Entropy for Ternary Amorphous Alloys, Mater. Trans. JIM. 41 (2000) 1372–1378. https://doi.org/10.2320/matertrans1989.41.1372.

[47] A. Takeuchi, A. Inoue, Classification of Bulk Metallic Glasses by Atomic Size Difference, Heat of Mixing and Period of Constituent Elements and Its

Application to Characterization of the Main Alloying Element, Mater. Trans. 46 (2005) 2817–2829. https://doi.org/10.2320/matertrans.46.2817.

[48] A.R. Miedema, On the heat of formation of solid alloys. II, J. Less-Common Met. 46 (1976) 67–83. https://doi.org/10.1016/0022-5088(76)90180-6.

[49] R. Boom, F.R. De Boer, A.R. Miedema, On the heat of mixing of liquid alloyS-II, J. Less-Common Met. 46 (1976) 271–284. https://doi.org/10.1016/0022-5088(76)90215-0.

[50] A.R. Miedema, F.R. de Boer, R. Boom, Model predictions for the enthalpy of formation of transition metal alloys, Calphad. 1 (1977) 341–359. https://doi.org/10.1016/0364-5916(77)90011-6.

[51] A.R. Miedema, R. Boom, F.R. De Boer, On the heat of formation of solid alloys, J. Less-Common Met. 41 (1975) 283–298. https://doi.org/10.1016/0022-5088(75)90034-X.

[52] A.R. Miedema, F.R. De Boer, R. Boom, Predicting heat effects in alloys, Phys. B+C. 103 (1981) 67–81. https://doi.org/10.1016/0378-4363(81)91003-2.

[53] K.S. Tun, A. Kumar, M. Gupta, Introducing a High Performance Mg-Based Multicomponent Alloy as an Alternative to Al-Alloys, Front. Mater. 6 (2019). https://doi.org/10.3389/fmats.2019.00215.

[54] L.J. Bannenberg, M. Heere, H. Benzidi, J. Montero, E.M. Dematteis, S. Suwarno, T. Jaroń, M. Winny, P.A. Orłowski, W. Wegner, A. Starobrat, K.J. Fijałkowski, W. Grochala, Z. Qian, J.P. Bonnet, I. Nuta, W. Lohstroh, C. Zlotea, O. Mounkachi, F. Cuevas, C. Chatillon, M. Latroche, M. Fichtner, M. Baricco, B.C. Hauback, A. El Kharbachi, Metal (boro-) hydrides for high energy density storage and relevant emerging technologies, Int. J. Hydrogen Energy. 45 (2020) 33687–33730. https://doi.org/10.1016/j.ijhydene.2020.08.119.

[55] G. Zepon, D.R. Leiva, R.B. Strozi, A. Bedoch, S.J.A. Figueroa, T.T. Ishikawa, W.J. Botta, Hydrogen-induced phase transition of MgZrTiFe0. 5Co0. 5Ni0. 5 high entropy alloy, Int. J. Hydrogen Energy. 43 (2018) 1702–1708.

[56] M.O. de Marco, Y. Li, H.-W. Li, K. Edalati, R. Floriano, Mechanical Synthesis and Hydrogen Storage Characterization of MgVCr and MgVTiCrFe High-Entropy Alloy, Adv. Eng. Mater. 22 (2020) 1901079.

[57] M.M. Nygård, G. Ek, D. Karlsson, M. Sahlberg, M.H. Sørby, B.C. Hauback, Hydrogen storage in high-entropy alloys with varying degree of local lattice strain, Int. J. Hydrogen Energy. 44 (2019) 29140–29149.

[58] T. Nagase, A. Terayama, T. Nagaoka, N. Fuyama, T. Sakamoto, Alloy Design and Fabrication of Ingots of Al–Mg–Li–Ca Light-Weight Medium Entropy Alloys, Mater. Trans. 61 (2020) 1369–1380. https://doi.org/10.2320/matertrans.F-M2020825.

[59] B. Cantor, Multicomponent and High Entropy Alloys, Entropy. 16 (2014) 4749–4768.

[60] M.C. Gao, P.K. Liaw, J.W. Yeh, Y. Zhang, High-entropy alloys: Fundamentals and applications, 2016. https://doi.org/10.1007/978-3-319-27013-5.